Received: 4 November 2019 | Revised: 8 April 2020 | Accepted: 16 June 2020

DOI: 10.4218/etrij.2019-0502

ORIGINAL ARTICLE

ETRI Journal WILEY

Walsh-Hadamard-transform-based SC-FDMA system using WARP hardware

Shri Ramtej Kondamuri | **Sundru Anuradha**

Department of Electronics and Communication Engineering, National Institute of Technology, Warangal, India

Correspondence
Shri Ramtej Kondamuri, Department of Electronics and Communication Engineering, National Institute of Technology, Warangal, Telangana, India.
Email: shriramtej@gmail.com

Abstract

Single-carrier frequency division multiple access (SC-FDMA) is currently being used in long-term evolution uplink communications owing to its low peak-to-average power ratio (PAPR). This study proposes a new transceiver design for an SC-FDMA system based on Walsh-Hadamard transform (WHT). The proposed WHT-based SC-FDMA system has low-PAPR and better bit-error rate (BER) performance compared with the conventional SC-FDMA system. The WHT-based SC-FDMA transmitter has the same complexity as that of discrete Fourier transform (DFT)-based transmitter, while the receiver's complexity is higher than that of the DFT-based receiver. The exponential companding technique is used to reduce its PAPR without degrading its BER. Moreover, the performances of different ordered WHT systems have been studied in additive white Gaussian noise and multipath fading environments. The proposed system has been verified experimentally by considering a real-time channel with the help of wireless open-access research platform hardware. The supremacy of the proposed transceiver is demonstrated based on simulated and experimental results.

KEYWORDS

companding technique, OFDM and multi-carrier systems, PAPR, real-time channels, SC-FDMA, WARP, WHT

1 | INTRODUCTION

The lower envelope fluctuations in single-carrier frequency-division multiple access (SC-FDMA) signals yield low peak-to-average power ratios (PAPRs). Thus, SC-FDMA is currently being used in long-term evolution (LTE) uplink communications [1]. However, PAPR increases in SC-FDMA systems when the modulation order is increased. To sustain high PAPR, power amplifiers with a large linear range are required and they reduce the power efficiency. Additionally, high-resolution analog-to-digital (A/D) and digital-to-analog (D/A) converters that increase system complexity and cost are required. This is a serious problem in uplink communications as the mobile devices are power limited [2]. Accordingly, the PAPR needs to be reduced.

In [3], authors presented sinusoidal transforms as an alternative to the discrete Fourier transform (DFT) for orthogonal frequency-division multiplexing (OFDM) systems. The energy compaction property of the discrete cosine transform (DCT) enables it to pack most of the signal energy in the first few samples, thus decreasing inter-symbol interference (ISI) due to relatively small amplitudes at high-frequency indices. This leads to a lower bit error rate (BER) compared with DFT. Furthermore, it uses real arithmetic operations instead of complex arithmetic

operations used in the DFT. This allowed authors in [4,5] to propose a new SC-FDMA system based on DCT Type II. In [6], authors demonstrated that the DCT SC-FDMA system is better than the DFT SC-FDMA system in terms of its BER performance. However, the PAPR of the DCT SC-FDMA system is slightly higher than that of the DFT SC-FDMA system. In [7], a new transceiver design for the SC-FDMA system based on discrete Wavelet transform (DWT) has been proposed. The DWT-based SC-FDMA system has superior BER and PAPR performances compared with the DFT SC-FDMA system. The Walsh-Hadamard Transform (WHT) is the most well-known nonsinusoidal orthogonal transform that can be computed using real additions and subtractions [8]. It has gained prominence in various digital signal processing applications, as its hardware implementation is simple. In [9], the application of WHT to generalized frequency-division multiplexing (GFDM) improved its BER performance. In [10], the application of WHT to non-orthogonal multiple access (NOMA) resulted in improved BER, throughput, and PAPR performances. As the application of various transforms improved the performance of SC-FDMA system, and the application of WHT improved the performances of GFDM and NOMA systems, this motivated us to study the performance of the WHT-based SC-FDMA transceiver.

Although there are many available techniques used to limit PAPR-like pulse shaping [11], selected mapping [12], partial transmit sequence [13], precoding [14], and predistortion [15], companding is an attractive technique with low complexity that does not require any side information. One of the most extensively used techniques to limit PAPR is μ-law companding [16]. The μ-law [17] and the new error function [18] companding techniques have been used to mitigate PAPR in SC-FDMA systems, but they increase the average power of the companded signal. In [19], authors proposed a companding technique to reduce the PAPR of the SC-FDMA signal by approximating its distribution without significant degradation in the BER performance. An exponential companding technique was used in [20] to reduce PAPR in OFDM systems without increasing the average power of the companded signal. Thus, we use the exponential companding technique in the WHT SC-FDMA system to reduce its PAPR without degrading the BER performance. Therefore, the main contributions of this study are as follows:

- The proposition of a new transceiver for a SC-FDMA system based on WHT and the use of exponential companding technique to reduce its PAPR without degrading the BER performance
- The derivation of the time-domain symbols for different ordered WHT systems
- The verification of the performance of proposed system by considering real-time indoor channel using wireless open-access research platform (WARP) hardware.

The rest of the study is organized as follows. Section 2 introduces the WHT and types of ordering in WHT. Section 3 explains the WHT-based SC-FDMA system model with the exponential companding technique. Section 4 explains how to select the optimum value of the companding parameter for better PAPR and BER performances, and presents the supremacy of the proposed transceiver through simulated PAPR and BER results. Section 5 presents the experimental results using WARP hardware. Section 6 outlines the conclusive comments of the study.

2 | WALSH-HADAMARD TRANSFORM

The WHT of a sequence is given by

$$\mathbf{X}_N = \frac{1}{N}\mathrm{H}_N\mathbf{x}_N \tag{1}$$

where H_N is a Hadamard matrix of order N, and $\mathbf{x}_N = [x_1,\ x_2,\ \ldots, x_N]^{\mathrm{T}}$ is an $N \times 1$ matrix. The Hadamard matrix of order N (where $N = 2^n$, n is a positive integer) can be defined recursively by using

$$\mathrm{H}_N = \begin{bmatrix} \mathrm{H}_{N/2} & \mathrm{H}_{N/2} \\ \mathrm{H}_{N/2} & -\mathrm{H}_{N/2} \end{bmatrix}, \tag{2}$$

where $\mathrm{H}_1 = [1]$. The WHT can also be defined as,

$$\mathrm{X}(u) = \frac{1}{N}\sum_{m=0}^{N-1} x(m)(-1)^{\langle m,\ u\rangle} u = 0, 1, \ldots, N-1, \tag{3}$$

$$\langle m,\ u\rangle = \sum_{s=0}^{n-1} u_s m_s;\ n = \log_2 N. \tag{4}$$

The terms u_s and m_s are the coefficients of the binary representations of u and m, respectively. The IWHT is defined as

$$x(m) = \sum_{u=0}^{N-1} \mathrm{X}(u)(-1)^{\langle m,\ u\rangle} m = 0, 1, \ldots, N-1. \tag{5}$$

2.1 | Types of ordering in WHT

There are three different ordering schemes used to compute the WHT, namely the Hadamard, Sequency, and Dyadic schemes [21]. The Hadamard-ordered (or Natural-ordered Hadamard) matrix of order eight is defined by using a recursive relation in (2) as.

$$(H_8)_h = \begin{bmatrix} 1 & 1 & 1 & 1 & 1 & 1 & 1 & 1 \\ 1 & -1 & 1 & -1 & 1 & -1 & 1 & -1 \\ 1 & 1 & -1 & -1 & 1 & 1 & -1 & -1 \\ 1 & -1 & -1 & 1 & -1 & -1 & -1 & 1 \\ 1 & 1 & 1 & 1 & -1 & -1 & -1 & -1 \\ 1 & -1 & 1 & -1 & -1 & 1 & -1 & 1 \\ 1 & 1 & -1 & -1 & -1 & -1 & 1 & 1 \\ 1 & -1 & -1 & 1 & -1 & 1 & 1 & -1 \end{bmatrix} \begin{matrix} 0 \\ 7 \\ 3 \\ 4 \\ 1 \\ 6 \\ 2 \\ 5 \end{matrix} \quad (6)$$

# of sign changes.

It is called natural order as **H** is not ordered based on the number of sign changes in each row. If **H** is ordered based on the number of sign changes, then we obtain the Sequency-ordered matrix as

$$(\mathrm{H}_8)_s = \begin{bmatrix} 1 & 1 & 1 & 1 & 1 & 1 & 1 & 1 \\ 1 & 1 & 1 & 1 & -1 & -1 & -1 & -1 \\ 1 & 1 & -1 & -1 & -1 & -1 & 1 & 1 \\ 1 & 1 & -1 & -1 & 1 & 1 & -1 & -1 \\ 1 & -1 & -1 & 1 & -1 & -1 & -1 & 1 \\ 1 & -1 & -1 & 1 & -1 & 1 & 1 & -1 \\ 1 & -1 & 1 & -1 & -1 & 1 & -1 & 1 \\ 1 & -1 & 1 & -1 & 1 & -1 & 1 & -1 \end{bmatrix} \begin{matrix} 0 \\ 1 \\ 2 \\ 3 \\ 4 \\ 5 \\ 6 \\ 7 \end{matrix} \quad (7)$$

# of sign changes.

The Dyadic-ordered matrix can be ordered by using the Gray code. The relation between the Sequency-ordered and Dyadic-ordered Walsh functions is given in Table 1. Herein, $b(i)$ represents the Gray code-to-binary conversion of i.

Thus, the Dyadic-ordered matrix arranges the sign changes in the order of 0, 1, 3, 2, 7, 6, 4, 5, as defined in (8),

$$(\mathrm{H}_8)_d = \begin{bmatrix} 1 & 1 & 1 & 1 & 1 & 1 & 1 & 1 \\ 1 & 1 & 1 & 1 & -1 & -1 & -1 & -1 \\ 1 & 1 & -1 & -1 & 1 & 1 & -1 & -1 \\ 1 & 1 & -1 & -1 & -1 & -1 & 1 & 1 \\ 1 & -1 & 1 & -1 & 1 & -1 & 1 & -1 \\ 1 & -1 & 1 & -1 & -1 & 1 & -1 & 1 \\ 1 & -1 & -1 & 1 & 1 & -1 & -1 & 1 \\ 1 & -1 & -1 & 1 & -1 & 1 & 1 & -1 \end{bmatrix} \begin{matrix} 0 \\ 1 \\ 3 \\ 2 \\ 7 \\ 6 \\ 4 \\ 5 \end{matrix} \quad (8)$$

# of sign changes.

3 | WHT-BASED SC-FDMA SYSTEM MODEL WITH EXPONENTIAL COMPANDING

The proposed WHT-based SC-FDMA transceiver with exponential companding is depicted in Figure 1. Input symbols are encoded and mapped to the complex symbols by any of the modulation techniques (BPSK, QPSK, or M-QAM), and passed through N-point WHT to obtain $\mathbf{X}_N$. The resultant N symbols are mapped to M subcarriers ($M = Q \times N$, $M > N$).

TABLE 1 Relation between Sequency- and Dyadic-ordered Walsh functions

i (decimal)	i (binary)	$b(i)$ (binary)	$b(i)$ (decimal)
0	000	000	0
1	001	001	1
2	010	011	3
3	011	010	2
4	100	111	7
5	101	110	6
6	110	100	4
7	111	101	5

For subcarrier mapping, there are two choices, namely, localized FDMA (LFDMA) and interleaved FDMA (IFDMA). In LFDMA, the symbols are mapped over consecutive subcarriers, and in IFDMA, the symbols are spread equidistantly over the entire bandwidth with zeros in between. $\mathbf{X}_N$ is mapped to $\mathbf{Y}_M$ (where $M = Q \times N$) as

$$\mathbf{Y}_M = \mathbf{M}\mathbf{X}_N, \quad (9)$$

For localized mapping

$$\mathbf{M} = \left[\mathbf{I}_N; 0_{(M-N)\times N}\right]. \quad (10)$$

For interleaved mapping

$$\mathbf{M} = \left[\mathbf{u}_1^{\mathrm{T}}; 0_{(Q-1)\times N}, \mathbf{u}_2^{\mathrm{T}}; 0_{(Q-1)\times N}, \ldots, \mathbf{u}_N^{\mathrm{T}}; 0_{(Q-1)\times N}\right], \quad (11)$$

where $\mathbf{I}_N$ is an $N \times N$ identity matrix, $0_{(Q-1)\times N}$ is a $(Q-1) \times N$ all-zero matrix, and $\mathbf{u}_l (l = 1, 2, \ldots, N)$ is a unit column vector of length N, with all-zero entries except at l. After subcarrier mapping, $\mathbf{Y}_M$ is passed through an M-point IWHT to obtain the time-domain signal given by

$$\begin{aligned} \mathbf{y}_M &= M\mathbf{H}_M^{-1}\mathbf{Y}_M, \\ \mathbf{y}_M &= \frac{M}{N}\mathbf{H}_M^{-1}\mathbf{M}\mathbf{H}_N\mathbf{x}_N, \end{aligned} \quad (12)$$

where $\mathbf{x}_N$ is an $N \times 1$ matrix of modulated symbols, $\mathbf{H}_N$ is an $N \times N$ WHT matrix, $\mathbf{M}$ is an $M \times N$ matrix describing the subcarrier mapping, and $\mathbf{H}_M^{-1}$ is an $M \times M$ IWHT matrix.

3.1 | Time-domain symbols

Considering the Hadamard-ordered WHT with $N = 2$, $M = 4$, $Q = 2$ and modulated symbols $\mathbf{x}_N = [x_1, x_2]^{\mathrm{T}}$, we have

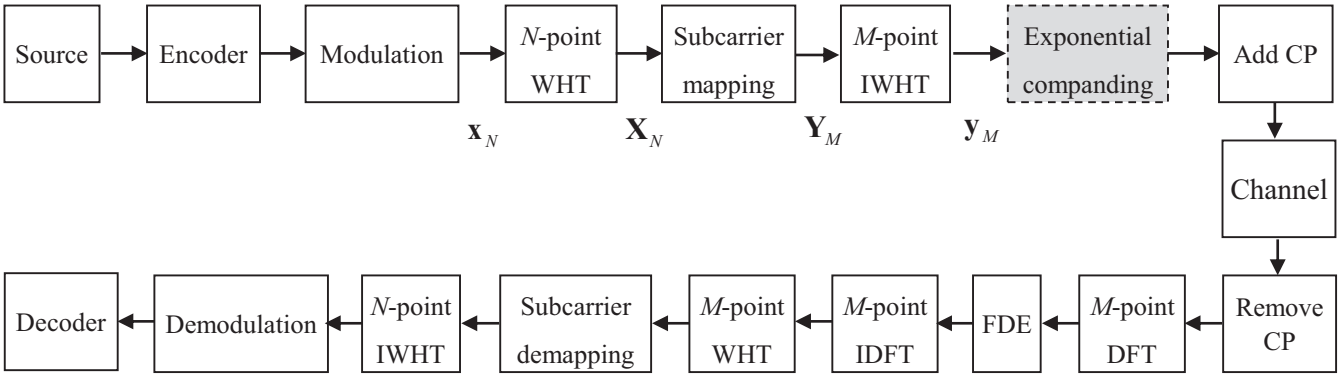

FIGURE 1 Walsh-Hadamard transform single-carrier frequency-division multiple access (WHT SC-FDMA) system with exponential companding

$$\mathbf{X}_N = \frac{1}{N}\mathrm{H}_N\mathbf{x}_N = \frac{1}{2}\begin{bmatrix}1 & 1\\ 1 & -1\end{bmatrix}\begin{bmatrix}x_1\\ x_2\end{bmatrix} = \begin{bmatrix}(x_1+x_2)/2\\ (x_1-x_2)/2\end{bmatrix}. \quad (13)$$

For localized mapping,

$$\mathbf{Y}_M = \mathbf{M}\mathbf{X}_N = \begin{bmatrix}1 & 0\\ 0 & 1\\ 0 & 0\\ 0 & 0\end{bmatrix}\begin{bmatrix}(x_1+x_2)/2\\ (x_1-x_2)/2\end{bmatrix} = \begin{bmatrix}(x_1+x_2)/2\\ (x_1-x_2)/2\\ 0\\ 0\end{bmatrix}, \quad (14)$$

$$\begin{aligned}\mathbf{y}_M &= M\mathbf{H}_M^{-1}\mathbf{Y}_M\\ &= 4\begin{bmatrix}1 & 1 & 1 & 1\\ 1 & -1 & 1 & -1\\ 1 & 1 & -1 & -1\\ 1 & -1 & -1 & 1\end{bmatrix}^{-1}\begin{bmatrix}(x_1+x_2)/2\\ (x_1-x_2)/2\\ 0\\ 0\end{bmatrix} = \begin{bmatrix}x_1\\ x_2\\ x_1\\ x_2\end{bmatrix}.\end{aligned} \quad (15)$$

Hence, for localized mapping $\mathbf{y}_M = [x_1, x_2, \ldots, x_N, x_1, x_2, \ldots, x_N, \ldots, x_1, x_2, \ldots, x_N]^{\mathrm{T}}$, that is, $\mathbf{x}_N$ will be repeated Q times. As the resulting WHT LFDMA symbols simply consist of modulated symbols in contrast with that of the DFT LFDMA symbols which consist of the sum of modulated symbols with different complex weights, the PAPR of the WHT LFDMA system will be smaller compared with the DFT LFDMA system. For interleaved mapping,

$$\mathbf{Y}_M = \mathbf{M}\mathbf{X}_N = \begin{bmatrix}1 & 0\\ 0 & 0\\ 0 & 1\\ 0 & 0\end{bmatrix}\begin{bmatrix}(x_1+x_2)/2\\ (x_1-x_2)/2\end{bmatrix} = \begin{bmatrix}(x_1+x_2)/2\\ 0\\ (x_1-x_2)/2\\ 0\end{bmatrix}, \quad (16)$$

$$\begin{aligned}\mathbf{y}_M &= M\mathbf{H}_M^{-1}\mathbf{Y}_M\\ &= 4\begin{bmatrix}1 & 1 & 1 & 1\\ 1 & -1 & 1 & -1\\ 1 & 1 & -1 & -1\\ 1 & -1 & -1 & 1\end{bmatrix}^{-1}\begin{bmatrix}(x_1+x_2)/2\\ 0\\ (x_1-x_2)/2\\ 0\end{bmatrix} = \begin{bmatrix}x_1\\ x_1\\ x_2\\ x_2\end{bmatrix}.\end{aligned} \quad (17)$$

Hence, for interleaved mapping $\mathbf{y}_M = [x_1, x_1, \ldots, x_1, x_2, x_2, \ldots, x_2, \ldots, x_N, x_N, \ldots, x_N]^{\mathrm{T}}$, that is, $x_1, x_2, \ldots$, and x_N will be repeated Q times. As the resulting WHT IFDMA symbols simply consists of modulated symbols similar to the DFT IFDMA symbols, the PAPR of the WHT IFDMA system will be same as that of the DFT IFDMA system.

Similarly, for Sequency-ordered WHT, the time-domain signal for localized mapping is given by

$$\mathbf{y}_M = \left[x_1, x_1, \ldots, x_1, x_2, x_2, \ldots, x_2, \ldots, x_N, x_N, \ldots, x_N\right]^{\mathrm{T}}, \quad (18)$$

That is, x_1, x_2, …, and x_N will be repeated Q times. For interleaved mapping

$$\mathbf{y}_M = \left[x_1, x_2, \ldots, x_N, x_N, x_{N-1}, \ldots, x_1, \ldots, x_1, x_2, \ldots, x_N\right]^{\mathrm{T}}. \quad (19)$$

For Dyadic-ordered WHT, the time-domain signal for localized mapping is given by

$$\mathbf{y}_M = \left[x_1, x_1, \ldots, x_1, x_2, x_2, \ldots, x_2, \ldots, x_N, x_N, \ldots, x_N\right]^{\mathrm{T}}, \quad (20)$$

That is, x_1, x_2, …, and x_N will be repeated Q times. For interleaved mapping,

$$\mathbf{y}_M = \left[x_1, x_2, \ldots, x_N, x_1, x_2, \ldots, x_N, \ldots, x_1, x_2, \ldots, x_N\right]^{\mathrm{T}}, \quad (21)$$

That is, $\mathbf{x}_N$ will be repeated Q times. As all the time-domain signals are simply the repetitions of modulated symbols, the PAPR values of the Hadamard-, Sequency-, and Dyadic-ordered WHT systems remain the same. Additionally, we can observe that the H-WHT with localized mapping and D-WHT with interleaved mapping are associated with the same time-domain signals. Similarly, the H-WHT with interleaved mapping, S-WHT, and D-WHT with localized mapping, all process the same time-domain signals. Hence, they tend to yield similar BER performances.

In turn, $\mathbf{y}_M$ is passed through an exponential compander to produce $\mathbf{t}_M$, where $\mathbf{t}_M = \left[\mathrm{t}_1, \mathrm{t}_2, \ldots, \mathrm{t}_M\right]^{\mathrm{T}}$. The companding operation can be described as.

$$t_m = h(y_m), \tag{22}$$

where y_m is the original signal, t_m is the companded signal, and $h(\cdot)$ is the companding function. The exponential companding function [17] is given by.

$$h(x) = \text{sgn}(x)\sqrt[d]{A\left[1 - \exp\left(-\frac{|x|^2}{\sigma^2}\right)\right]}, \tag{23}$$

where sgn(.) is the sign function and d controls the amount of companding. A maintains the average power of output signal at the same level as that of the input signal.

$$A = \left(\frac{E\left[|x|^2\right]}{E\left[\sqrt[d]{\left[1 - \exp\left(-\frac{|x|^2}{\sigma^2}\right)\right]^2}\right]}\right)^{\frac{d}{2}}. \tag{24}$$

At the receiver side, the decompanding function is given by

$$h^{-1}(x) = \text{sgn}(x)\left|\sqrt{-\sigma^2 \log_e\left(1 - \frac{|x|^d}{A}\right)}\right|. \tag{25}$$

The cyclic prefix (CP) is then added to t_m and transmitted over the wireless channel. CP is removed at the receiver side and is transformed via an M-point DFT for frequency-domain equalization (FDE). It is then inverted back to the time-domain by using M-point IDFT. The corresponding inverse operations, like M-point WHT, subcarrier demapping, N-point IWHT, demodulation, and decoding operations, are performed to retrieve the source data.

3.2 | No decompanding (NDC)

The companded signal, t_m can be expressed in terms of companding noise, b_m and input signal, y_m as

$$t_m = \alpha y_m + b_m, \tag{26}$$

where α is the attenuation factor given by [22]

$$\alpha = \frac{E\left\{t_m y_m^*\right\}}{E\left\{y_m y_m^*\right\}}. \tag{27}$$

From (26), $P_{t_m} = P_{\alpha y_m} + P_{b_m} = \alpha^2 P_{y_m} + P_{b_m}$, where P is the average power. As t_m and y_m have the same average power

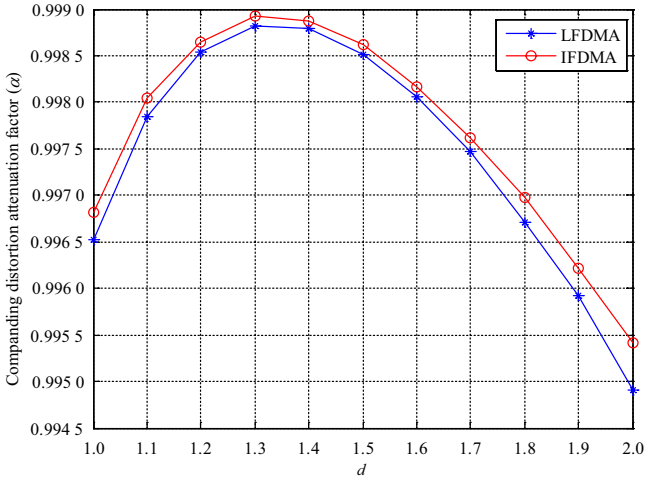

FIGURE 2 Companding distortion attenuation factor of exponential companding scheme

$$\begin{aligned} P_{t_m} &= P_{y_m}, \\ \alpha^2 P_{y_m} + P_{b_m} &= P_{y_m}, \\ P_{b_m} &= \left(1 - \alpha^2\right) P_{y_m}. \end{aligned} \tag{28}$$

Based on the above equations, it can be inferred that α will always be less than one, and the companding noise will reduce as α tends to 1. The received signal, r_m in the presence of channel noise, w_m can be expressed as

$$r_m = t_m + w_m. \tag{29}$$

The recovered signal, y'_m after the decompanding operation can be written as

$$y'_m = \frac{r_m - b_m}{\alpha}. \tag{30}$$

Simplifying (30) yields

$$y'_m = \frac{t_m + w_m - b_m}{\alpha} = \frac{t_m - b_m}{\alpha} + \frac{w_m}{\alpha} = y_m + \frac{w_m}{\alpha}. \tag{31}$$

Equation (31) shows that the decompanding operation amplifies the channel noise from w_m to w_m/α. Therefore, the equivalent noise without and with the decompanding operation can be written as $b_m + w_m$ and w_m/α, respectively. Figure 2 shows the plot of the attenuation factor α vs. d for the exponential companding scheme. From (28), as α tends to one, the power of companding noise will decrease, and the BER performance of the system will be improved. The values of α for the proposed LFDMA and IFDMA systems were respectively evaluated to be 0.998 8 and 0.998 9 (close to 1) for $d = 1.3$. Hence, we can say that the proposed method yields a very low level of companding noise when $d = 1.3$. Thus, the proposed system with NDC can also provide a decent BER performance.

3.3 | Complexity evaluation

The fast WHT algorithm in [8] has a similar computational complexity as that of the fast DFT algorithm. Similar to the DFT, the fast WHT requires $N\log_2 N$ arithmetic operations for N-point sequences. Hence, the WHT-based SC-FDMA transmitter has comparative complexity to that of the DFT-based transmitter. The receiver's complexity is slightly higher than that of the DFT-based receiver, as it uses additional DFT and IDFT blocks for frequency-domain equalization. Therefore, it requires additional $2N\log_2 N$ arithmetic operations at the receiver side compared with the DFT-based receiver. However, as the receiver is a base station in case of uplink communications, a slightly higher complexity can be accepted owing to the supremacy of the WHT-based SC-FDMA system.

4 | PERFORMANCE ANALYSIS

The efficiency of the proposed system presented in Figure 1 has been evaluated by considering N = 128, M = 512, 16-quadrature amplitude modulation (QAM), and localized

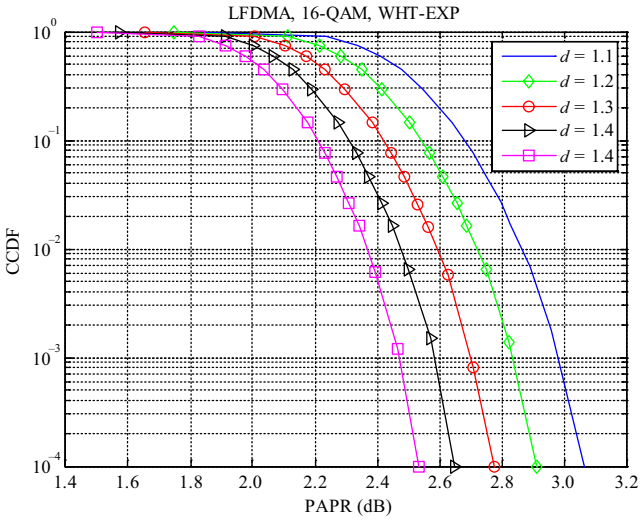

FIGURE 3 Complementary cumulative distribution function (CCDF) curves of the proposed system with localized FDMA (LFDMA) for different values of d

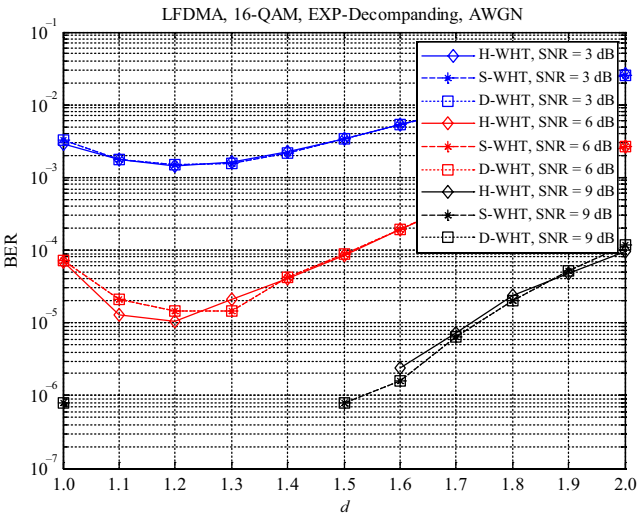

FIGURE 5 Plots of bit-error rate (BER) as a function of d for the proposed LFDMA system with decompanding for different signal-to-noise ratio (SNR)

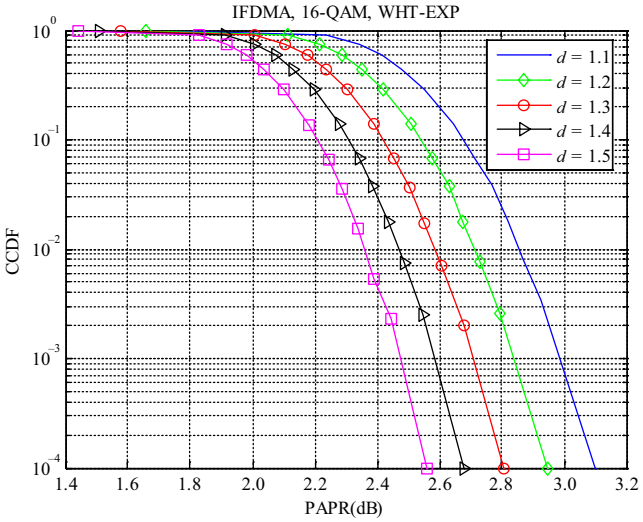

FIGURE 4 CCDF curves of the proposed system with interleaved FDMA (IFDMA) for different values of d

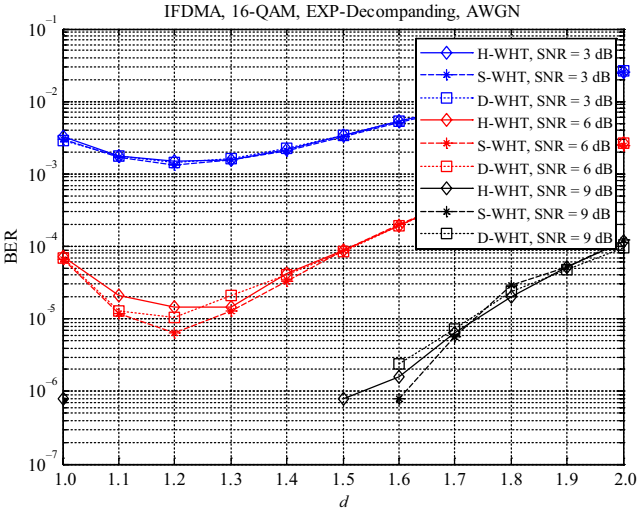

FIGURE 6 Plots of BER as a function of d for the proposed IFDMA system with decompanding for different SNR

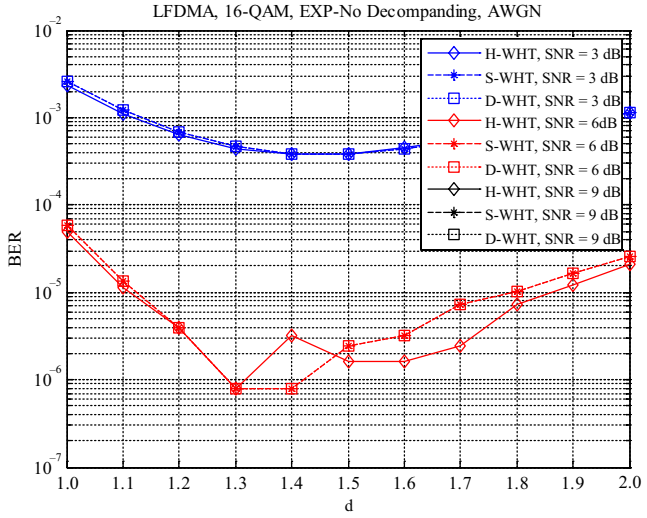

FIGURE 7 Plots of BER as a function of d for the proposed LFDMA system with no decompanding for different SNR

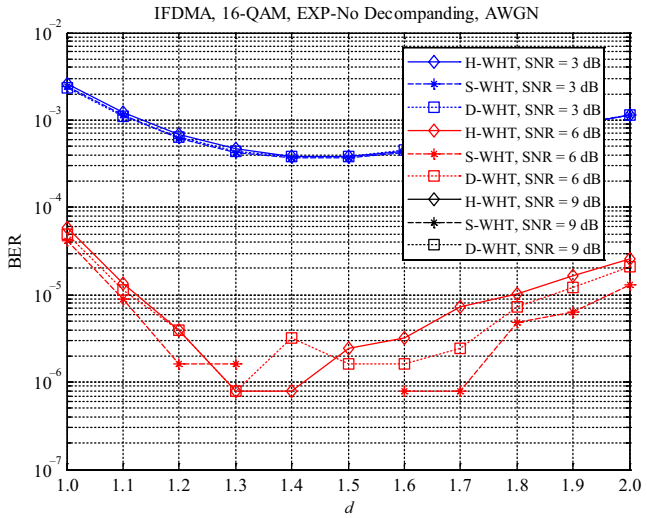

FIGURE 8 Plots of BER as a function of d for the proposed IFDMA system with no decompanding for different SNR

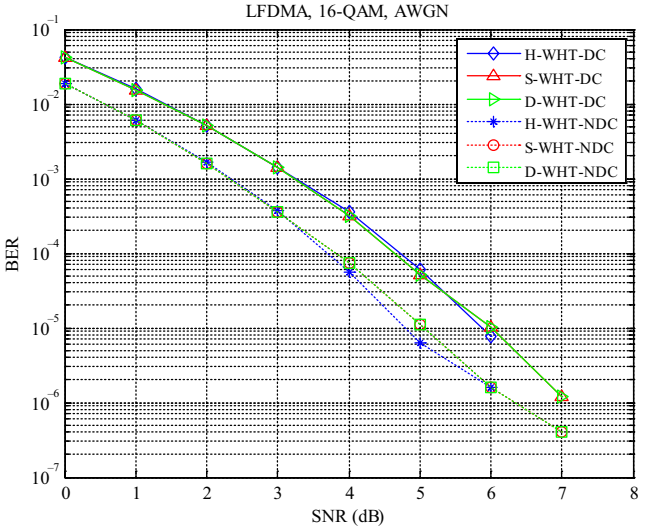

FIGURE 9 BER performance comparison of the proposed LFDMA system with decompanding (DC) and no decompanding (NDC)

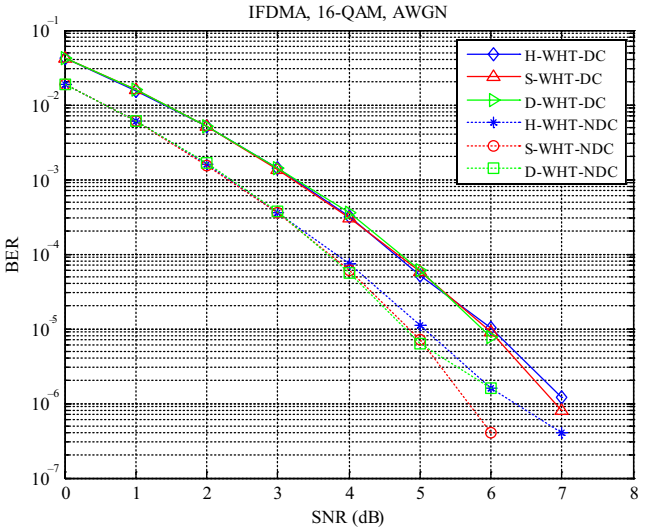

FIGURE 10 BER performance comparison of the proposed IFDMA system with DC and NDC

and interleaved subcarrier mapping techniques. A CP of 20 samples, and a convolutional channel coding with a rate of 1/2 was used. We have used perfect channel estimation with zero forcing (ZF) equalization.

Figures 3 and 4 present the complementary cumulative distribution function (CCDF) curves of the exponential companding technique with localized and interleaved mapping for various d values, respectively. It can be observed that PAPR has been reduced by approximately 0.6 dB at CCDF = 10^{-4} as d increases from 1.1 to 1.5.

BER plots as a function of d are depicted in Figures 5 and 6, respectively, for the proposed LFDMA and IFDMA systems with decompanding (DC) operations for various SNRs. Herein, H, S, D refer to Hadamard, Sequency, and Dyadic ordering of the WHT, respectively. It can be noted that $d = 1.2$ is the optimum value for lower BER in all cases.

Corresponding BER plots as a function of d for the proposed LFDMA and IFDMA systems with NDC operation for various SNRs are illustrated in Figures 7 and 8, respectively. It can be observed that $d = 1.3$ is the optimum value for the system with no decompanding operation. It is also evident from Figure 2 that companding noise is minimized when $d = 1.3$. Considering both the CCDF and BER plots, $d = 1.2$ and 1.3 can be chosen as the optimum values for the proposed system with DC and NDC, respectively, to achieve a trade-off between the BER and PAPR performances.

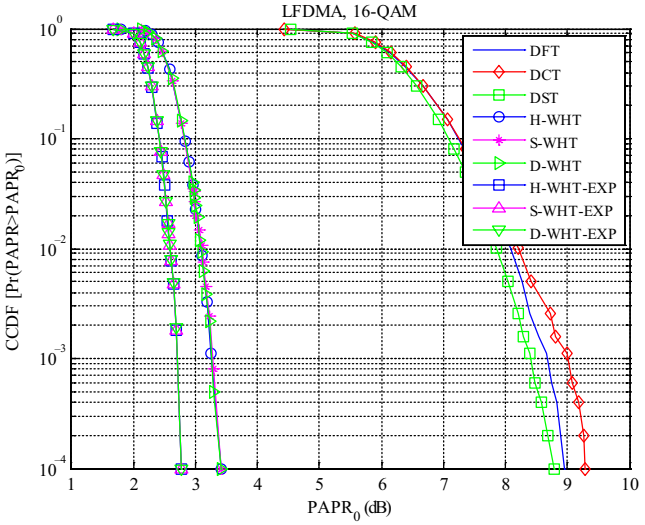

FIGURE 11 CCDF curves of different systems with localized mapping

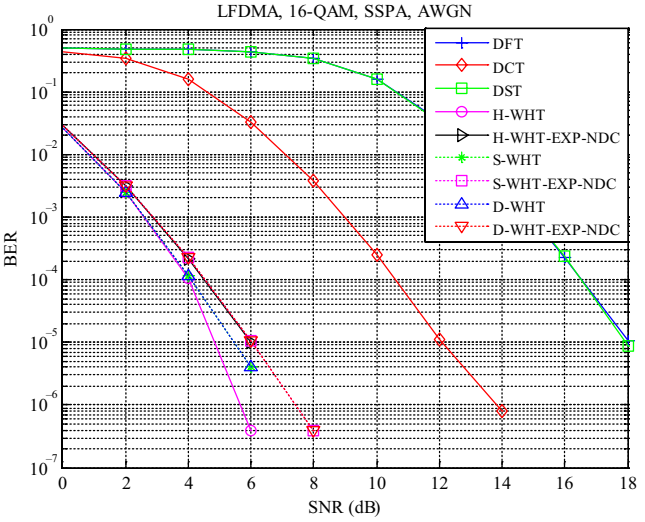

FIGURE 13 BER curves of various LFDMA systems in the additive white Gaussian noise (AWGN) channel with solid state power amplifier (SSPA) (p = 2, IBO = 5 dB)

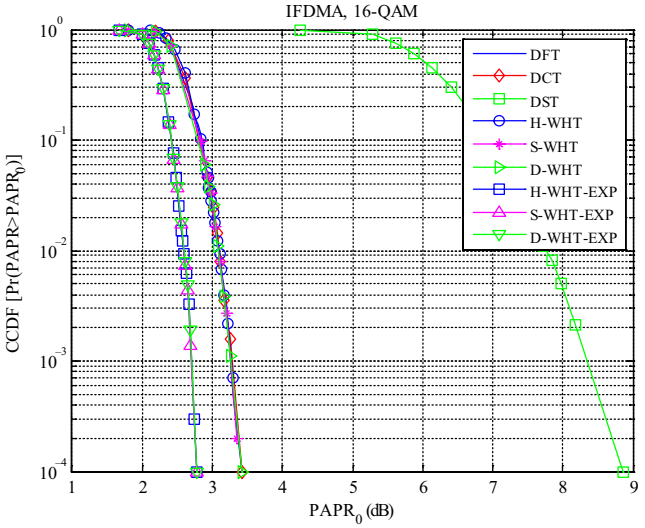

FIGURE 12 CCDF curves of different systems with interleaved mapping

Comparison of the BER curves of the proposed system with DC and NDC operations for localized and interleaved mapping techniques are presented in Figures 9 and 10, respectively. It can be observed that the system with NDC has a performance SNR gain of 1 dB compared with the system with DC in both cases.

CCDF curves of DFT, DCT, Discrete Sine Transform (DST), and WHT-based SC-FDMA systems for localized and interleaved mapping techniques are shown in Figures 11 and 12, respectively. For localized mapping, we can observe that the DCT-based system has high PAPR, and the DST-based system has a low PAPR compared with the DFT-based system. The proposed WHT-based system has a low PAPR compared with the DFT, DCT, and DST-based systems. We can also observe that the Hadamard, Sequency, and Dyadic-ordered WHT systems provide the same PAPR, as discussed in Section 3.1. When exponential companding is used in the WHT-based system, PAPR improves further.

For interleaved mapping, it can be observed that the DFT, DCT, and WHT-based systems provide the same PAPR. From Figures 11 and 12, we can also conclude that the WHT-based system provides the same PAPR for both localized and interleaved mapping methods. Table 2 summarizes the values of PAPR for different systems at CCDF = 10^{-4}. Table 2 listings indicate that the proposed WHT-based system reduces PAPR by approximately 5.51 dB at CCDF = 10^{-4}, while WHT-EXP reduces PAPR by approximately 6.12 dB when compared with the DFT-based system when localized mapping is used.

The BER performance curves of DFT, DCT, DST, and WHT-based SC-FDMA systems in the AWGN channel for localized and interleaved mapping techniques by considering a solid state power amplifier (SSPA) with IBO = 5 dB and p = 2 [23] are shown in Figures 13 and 14 respectively. We can observe that all the Hadamard-, Sequency-, and

TABLE 2 Peak-to-average power ratio (PAPR) values in dB at CCDF = 10^{-4}

	DFT	DCT	DST	H-WHT	S-WHT	D-WHT	H-WHT-EXP	S-WHT-EXP	D-WHT-EXP
LFDMA	8.96	9.39	8.77	3.45	3.45	3.45	2.84	2.84	2.84
IFDMA	3.45	3.45	8.79	3.45	3.45	3.45	2.84	2.84	2.84

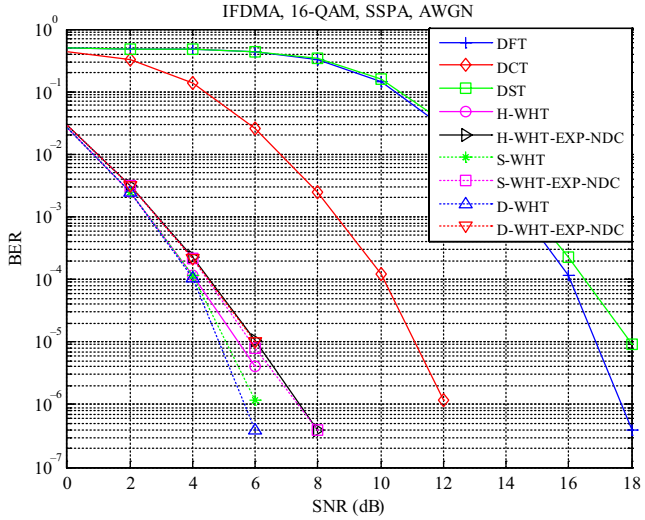

FIGURE 14 BER curves of various IFDMA systems in the AWGN channel with SSPA (p = 2, IBO = 5 dB)

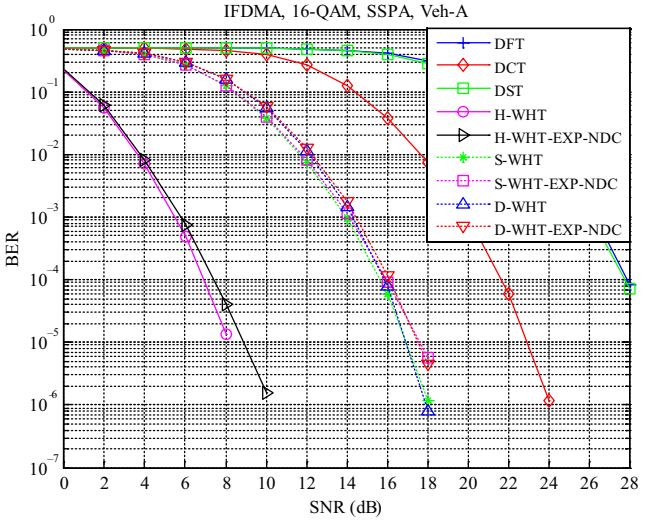

FIGURE 16 BER curves of various IFDMA systems in the Veh-A channel with SSPA (p = 2, IBO = 5 dB)

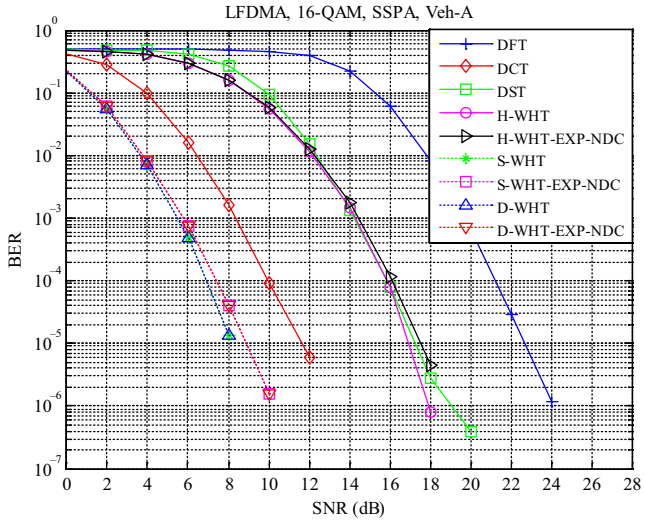

FIGURE 15 BER curves of various LFDMA systems in the Veh-A channel with SSPA (p = 2, IBO = 5 dB)

Dyadic-ordered WHT systems perform similarly. When exponential companding is used in the WHT-based system, we can observe that there is a slight degradation in the BER performance that is almost negligible.

BER performance curves of different systems in the Vehicular-A channel for localized and interleaved mapping techniques based on SSPA considerations are presented in Figures 15 and 16, respectively. Vehicular-A channel is used to model a multipath slow-fading frequency-selective Rayleigh channel [24]. We can observe that S-WHT and D-WHT systems provide better BER performances with localized mapping, whereas the H-WHT system provides better BER performance with interleaved mapping. Additionally, as stated in Section 3.1, H-WHT with localized mapping and D-WHT with interleaved mapping yields the same BER performance. H-WHT with interleaved mapping and S-WHT, D-WHT with localized mapping has the same BER performance. Table 3 shows the required SNR values to attain a BER of 10^{-4} in different systems.

5 | EXPERIMENTAL VALIDATION

WARP v3 hardware developed by Mango Communications (Houston, USA) is used to implement the experiments. The WARPLab framework [25] allows physical layer algorithms to be prototyped by combining the features of MATLAB (version R2013a, MathWorks, Natick, MA, USA) with the capabilities of WARP. The WARPLab framework allows MATLAB to control the WARP nodes and perform signal processing operations. The WARP repository [26] contains the necessary MATLAB m-code and

TABLE 3 Signal-to-noise ratio (SNR) values in dB required for BER = 10^{-4}

		DFT	DCT	DST	H-WHT	H-WHT-EXP	S-WHT	S-WHT-EXP	D-WHT	D-WHT-EXP
AWGN	LFDMA	17.18	11.27	17.21	4.13	5.15	4.25	5.16	4.25	5.16
	IFDMA	16.25	10.35	17.17	4.25	5.16	4.30	5.11	4.13	5.15
Veh-A	LFDMA	21.77	9.99	15.96	15.97	16.29	7.63	7.83	7.63	7.83
	IFDMA	27.97	21.91	27.95	7.63	7.83	15.91	15.98	15.97	16.29

FPGA code functions required for the interaction between the MATLAB workspace and the WARP nodes. A WARP node comprises two identical radiofrequency (RF) interfaces: RF A and RF B. Each RF interface has a transceiver operating at 2.4/5 GHz with an RF bandwidth of 40 MHz. RF A is used to transmit samples, and RF B is used to receive the samples.

A basic WARPLab setup where a WARP node and a host personal computer are connected via an Ethernet switch is used to verify the experiments. The baseband samples were constructed in MATLAB and the WARPLab framework downloaded the samples from the MATLAB workspace to the FPGA buffers. A trigger signal was sent from the host PC to the WARP node so that samples can be transmitted from RF A to RF B. The baseband samples are upconverted to the RF signal at the transmitter side and downconverted at the receiver side. These downconverted samples are then stored in buffers before they are loaded in the MATLAB workspace. These are then processed on the host PC with MATLAB.

The experimental setup of the proposed WHT-based SC-FDMA system using WARP v3 board is depicted in Figure 17. Initially, 1000 symbols of random data are generated, modulated, and corresponding operations of the SC-FDMA modulator are performed before adding CPs. Pilot symbols are then added and passed through a square-root raised cosine filter with a roll-off factor of 0.3. Subsequently, a preamble is added, and the baseband signal is upconverted to 5 MHz before its transmission over the air. The received signal is downconverted to a baseband signal and is correlated with the reference signal to detect the preamble sequence. The channel is estimated by using pilot symbols, and corresponding operations of SC-FDMA demodulator are performed. BER vs. transmit amplifier gain curves of the proposed WHT-based system and conventional system over real-time channel for localized and interleaved mapping techniques are presented in Figures 18 and 19, respectively. As the gain of the transmit amplifier increases, the strength of the transmitted signal increases hence decreasing the BER. It can be observed that all the Hadamard-, Sequency-, and Dyadic-ordered WHT-based SC-FDMA systems perform either better or maintain the performance of the conventional SC-FDMA system, but do not degrade the performance. Sequency-ordered WHT-based systems provide better BER performance with localized mapping, whereas the Hadamard-ordered WHT-based system provide better BER performance with interleaved mapping.

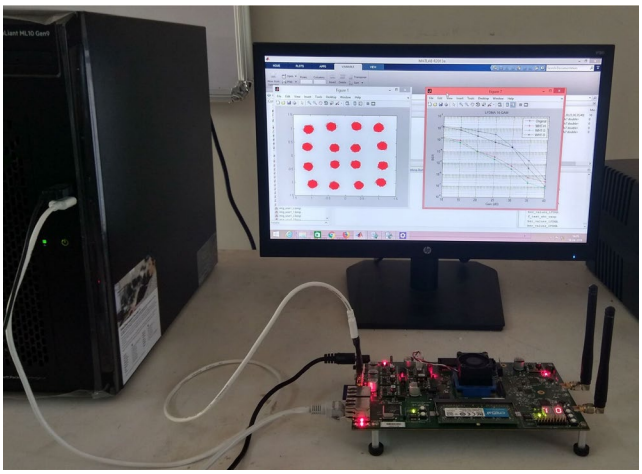

FIGURE 17 Experimental setup using the wireless open-access research platform (WARP) v3 board

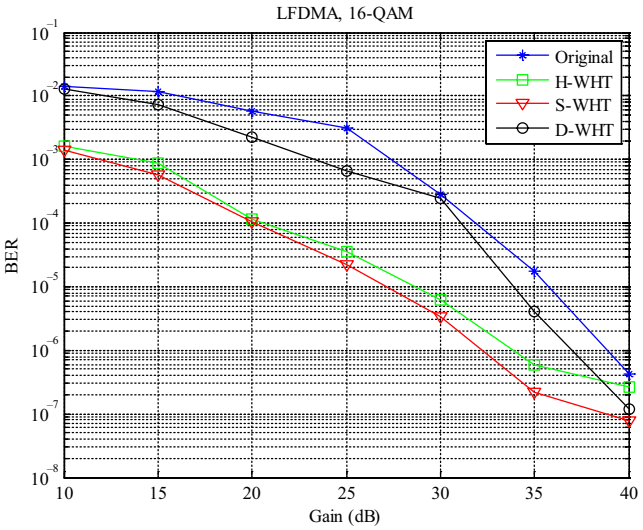

FIGURE 18 BER curves of various LFDMA systems in a real-time channel

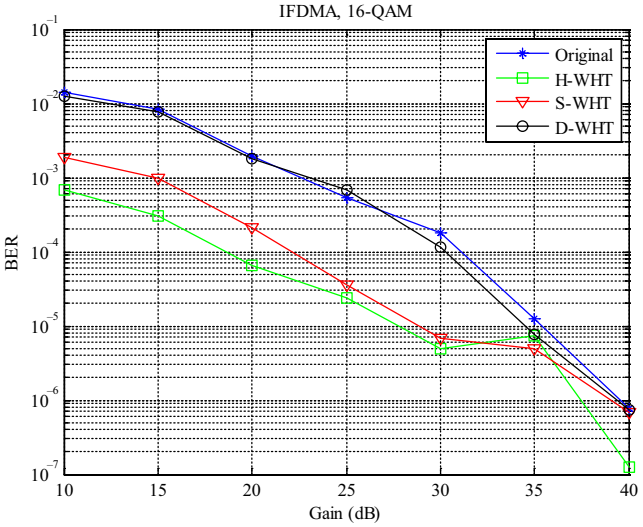

FIGURE 19 BER curves of various IFDMA systems in a real-time channel

6 | CONCLUSIONS

In this study, we proposed an SC-FDMA transceiver based on the WHT that offered low PAPR and better BER performance compared with a conventional DFT-based SC-FDMA system. The complexity of the proposed system was similar to the conventional system at the transmitter side, while the receiver complexity was slightly higher. The exponential companding technique with NDC operation has been used to reduce the PAPR value without degrading the BER performance. Hadamard-, Sequency-, and Dyadic-ordered systems perform similarly in the case of the AWGN channel. The Hadamard-ordered system performed well in the case of interleaved mapping and the Sequency-, Dyadic-ordered systems perform well in the case of localized mapping when the multipath fading environment was considered. The proposed WHT SC-FDMA system has also been verified experimentally by considering a real-time channel with the help of WARP hardware. Hence, the WHT-based SC-FDMA system can be used as an alternative to the conventional DFT-based SC-FDMA system in practice. We anticipate to study in more depth the throughput and spectral efficiency performances of the proposed system in the future.

CONFLICT OF INTEREST

On behalf of all authors, the corresponding author states that there are no conflicts of interest.

ORCID


Shri Ramtej Kondamuri https://orcid.org/0000-0003-0402-5806

REFERENCES

1. H. Myung, J. Lim, and D. Goodman, *Single carrier FDMA for uplink wireless transmission*, IEEE Veh. Technol. Mag. **1** (2006), 30–38.
2. G. Wunder et al., *The PAPR problem in OFDM transmission: New directions for a long-lasting problem*, IEEE Signal Process. Mag. **30** (2013), 130–144.
3. G. D. Mandyam, *Sinusoidal transforms in OFDM systems*, IEEE Trans. Broadcast. **50** (2004), 172–184.
4. F. S. Al-Kamali et al., *A new single carrier FDMA system based on the discrete cosine transform*, in Proc. Int. Conf. Comput. Eng. Syst. (Cairo, Egypt), 2009, pp. 555–560.
5. F. S. Al-Kamal et al., *An efficient transceiver scheme for SC-FDMA systems based on discrete wavelet transform and discrete cosine transform*, Wirel. Pers. Commun. **83** (2015), 3133–3155.
6. F. El-Samie et al., *SC-FDMA for mobile communications*, CRC Press, Taylor & Francis Group, Boca Raton, FL, 2014.
7. A. Khan et al., *Walsh Hadamard transform based transceiver design for SC-FDMA with discrete wavelet transform*, China Commun. **14** (2017), 193–206.
8. N. Ahmed and K. R. Rao, *Walsh-hadamard transform*, in Orthogonal Transforms for Digital Signal Processing, Springer, Berlin, Heidelberg, 1975. https://link.springer.com/chapter/10.1007/978-3-642-45450-9_6
9. N. Michailow et al., *Robust WHT-GFDM for the next generation of wireless networks*, IEEE Commun. Lett. **19** (2015), 106–109.
10. M. R. Usman et al., *Joint non-orthogonal multiple access (NOMA) & walsh-hadamard transform: Enhancing the receiver performance*, China Commun. **15** (2018), 160–177.
11. J. Ji, G. Ren, and H. Zhang, *PAPR reduction of SC-FDMA signals via probabilistic pulse shaping*, IEEE Trans. Veh. Technol. **64** (2015), 3999–4008.
12. A. Mohammad, A. Zekry, and F. Newagy, *A time domain SLM for PAPR reduction in SC-FDMA systems*, in Proc. IEEE Global High Tech. Congress Electron. (Shenzhen, China), 2012, pp. 143–147.
13. H. S. Joo et al., *New PTS schemes for PAPR reduction of OFDM signals without side information*, IEEE Trans. Broadcast. **63** (2017), 562–570.
14. C. H. G. Yuen, and B. Farhang-Boroujeny, *Analysis of the optimum precoder in SC-FDMA*, IEEE Trans. Wirel. Commun. **11** (2012), 4096–4107.
15. Y. Xia and J. Ji, *Reducing PAPR of SC-FDMA signals through simple amplitude predistortion*, ETRI J. **37** (2015), 922–928.
16. X. Wang, T. T. Tjhung, and C. S. Ng, *Reduction of peak-to-average power ratio of OFDM system using a companding technique*, IEEE Trans. Broadcast. **45** (1999), 303–307.
17. F. E. Abd El-Samie et al., *Performance enhancement of SC-FDMA systems using a companding technique*, Ann. Telecommun. **65** (2010), 293–300.
18. K. S. Ramtej and S. Anuradha, *New error function companding technique to minimize PAPR in LTE uplink communications*, in Proc. National Conf. Commun. (Chennai, India), 2017, pp. 1–5.
19. S. R. Kondamuri and A. Sundru, *Performance analysis of hybrid PAPR reduction technique for LTE uplink communications*, Phys. Commun. **29** (2018), 103–111.
20. T. Jiang, Y. Yang, and Y.-H. Y. H. Song, *Exponential companding technique for PAPR reduction in OFDM systems*, IEEE Trans. Broadcast. **51** (2005), 244–248.
21. Y. A. Geadah and M. J. G. Corinthios, *Natural, dyadic, and sequency order algorithms and processors for the Walsh-Hadamard transform*, IEEE Trans. Comput. **26** (1977), 435–442.
22. J. Hou et al., *Peak-to-average power ratio reduction of OFDM signals with nonlinear companding scheme*, IEEE Trans. Broadcast. **56** (2010), 258–262.
23. M. Hu et al., *Parameter-adjustable piecewise exponential companding scheme for peak-to-average power ratio reduction in orthogonal frequency division multiplexing systems*, IET Commun. **8** (2014), 530–536.
24. R. Jain, *Channel models: A tutorial*, WiMAX Forum AATG, 2007, pp. 1–21.
25. WARPLab framework, available from http://warpproject.org/trac/wiki/WARPLab.
26. WARP repository, available from http://warpproject.org/trac.

AUTHOR BIOGRAPHIES

Kondamuri Shri Ramtej received his BTech degree in Electronics and Communication Engineering from Jawaharlal Nehru Technological University, Hyderabad, Telangana, India, in 2012, and his MTech degree in communication systems and networks from the National Institute of Technology, Hamirpur, Himachal Pradesh, India, in 2014. He obtained his PhD degree in the area of wireless communications from the National Institute of Technology, Warangal, Telangana, India, in 2020. He is currently working as an Assistant Professor in the Department of Electronics and Communication Engineering at the Velagapudi Ramakrishna Siddhartha Engineering College, Vijayawada, Andhra Pradesh, India. His research interests include wireless communications and signal processing.

Sundru Anuradha received her BTech and MTech degrees in Electronics and Communication Engineering from the University of Nagarjuna, Guntur, Andhra Pradesh, India, in 1999, and the Sri Venkateswara University, Tirupati, Andhra Pradesh, India, in 2001, respectively. She obtained her PhD degree in Electronics and Communication Engineering from the Andhra University, Visakhapatnam, Andhra Pradesh, India, in 2012. She is currently an Associate Professor in the Department of Electronics and Communication Engineering at the National Institute of Technology, Warangal, Telangana, India. Her research interests include wireless communications, cognitive radio, antenna design and coding theory. She has more than 75 publications in various conferences and journals.